Electronic Supplementary Material (ESI) for Nanoscale.

Supporting Information

Mechanistic Elucidation of the Catalytic Activity of Silver Nanoclusters: Exploring the Predominant Role of Electrostatic Surface

Paritosh Mahato, Shashi Shekhar, Rahul Yadav and Saptarshi Mukherjee*

Department of Chemistry

Indian Institute of Science Education and Research Bhopal

Bhopal Bypass Road, Bhauri, Bhopal 462066, Madhya Pradesh, India

**Corresponding author: E-mail: saptarshi@iiserb.ac.in, Tel.: +91-755-269-1301.*

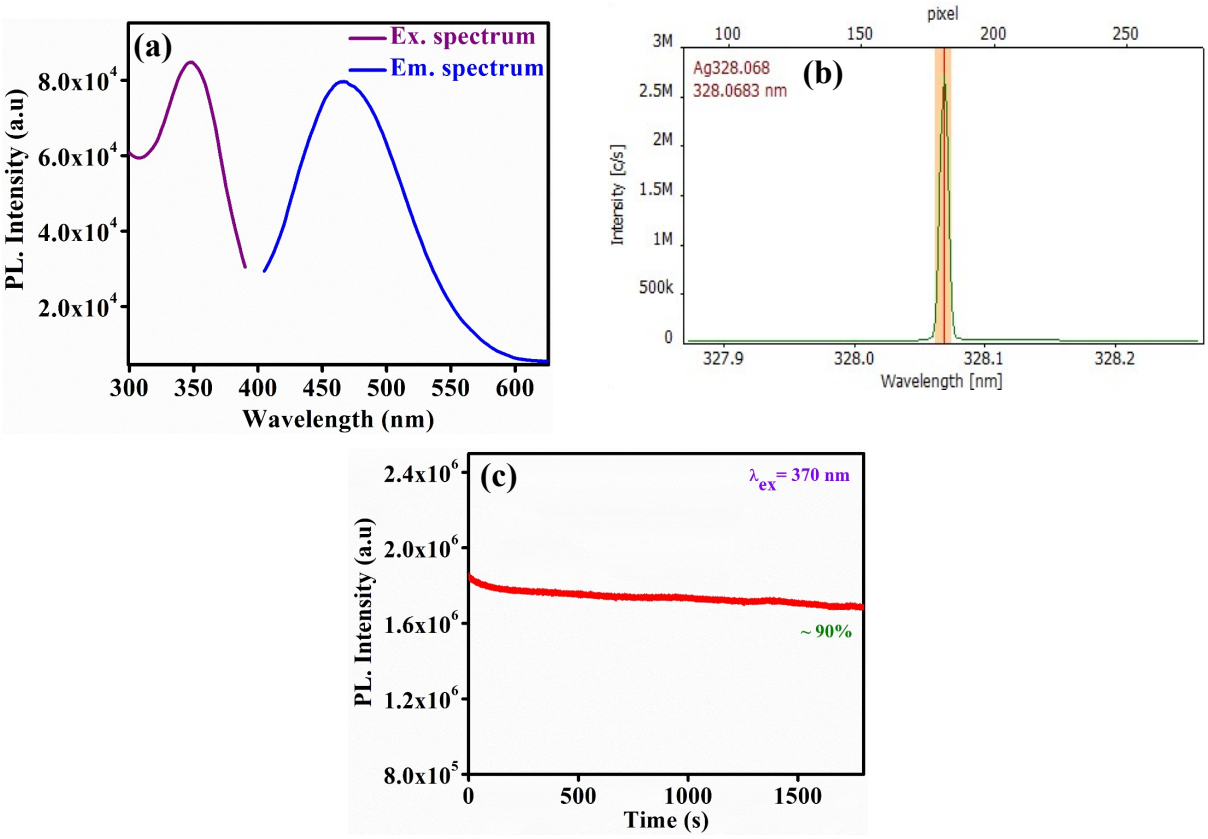

Fig. S1 (a) The un-normalized excitation and emission spectra of the MSA-templated AgNCs. (b) ICP-OES spectrum for Ag in 2% HNO_3 solution of AgNCs. (c) The photo-stability of Mg-AgNCs upon constant illumination (at 370 nm) from the excitation source.

Table S1: The Ag content in the solution of AgNCs.

Sample	Monitoring Spectra (nm)	Ag Content (ppm)
Standard Sample -5 ppm	Ag328.068	4.97 ± 0.1
AgNCs in 2% HNO_3	Ag328.068	18.08 ± 0.5

Calculation of the concentration of AgNCs from the ICP-OES studies:

For the ICP-OES studies, the sample was diluted by 6 times in which the Ag content was found to be 18.08 ppm. Hence the real content of Ag in the sock solution of the as-prepared AgNCs can be calculated by multiplying the dilution factors which was found to be 108.48 ppm. In our previous studies, we reported the composition of AgNCs as $Ag_4(MSA)_2$.[S1] So, the concentration of the AgNCs can be calculated as 108.48/ (4×107.8) = 252 μM which is in excellent agreement with our theoretical calculation i.e., 250 μM.

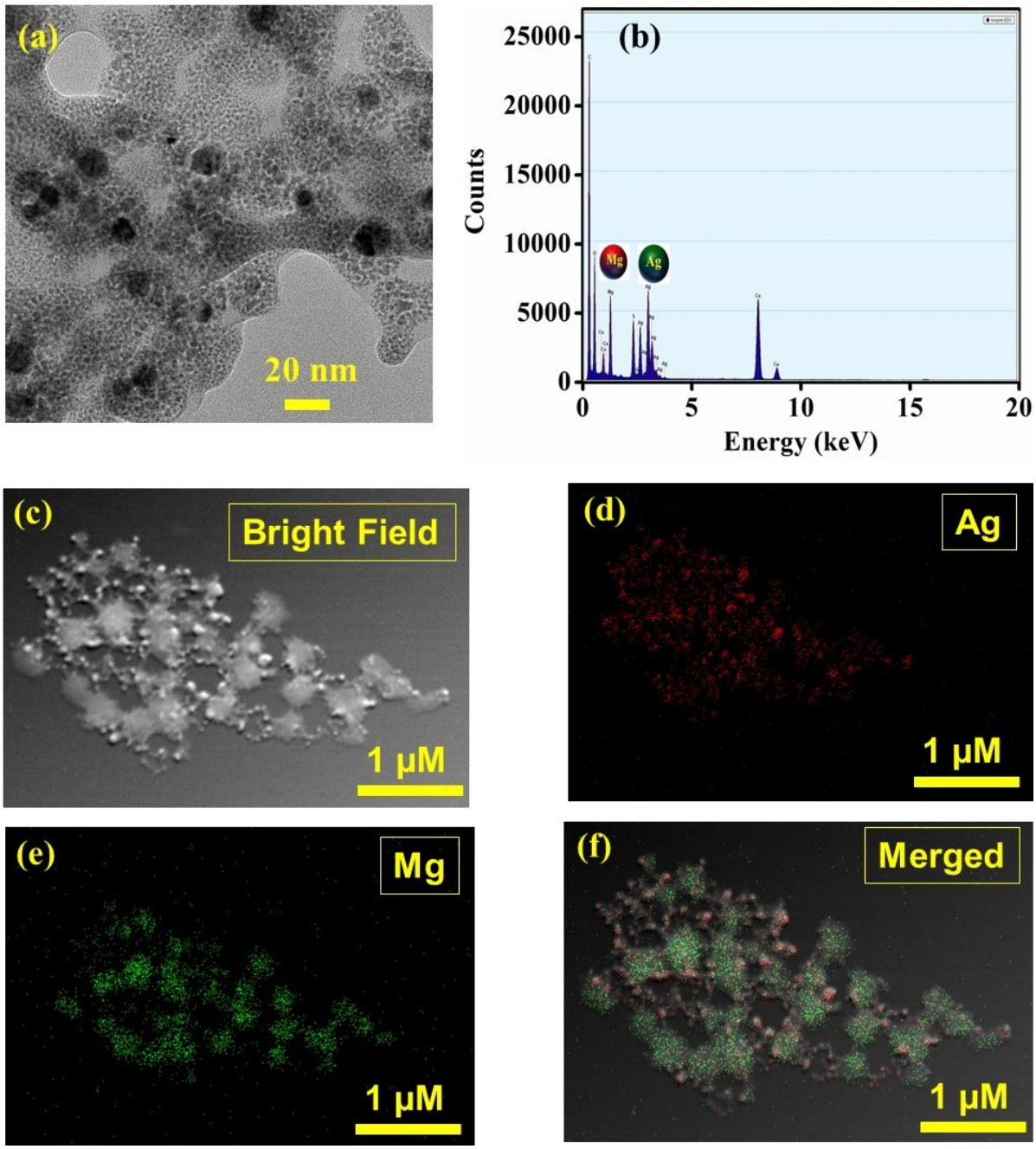

Fig. S2 (a) TEM image of Mg-AgNCs. (b) Corresponding elemental analysis showing the simultaneous presence of Ag and Mg. (c) Bright-field scanning TEM images of Mg-AgNCs. The elemental mapping for (d) Ag, (e) Mg, and (f) Merged in Mg-AgNCs.

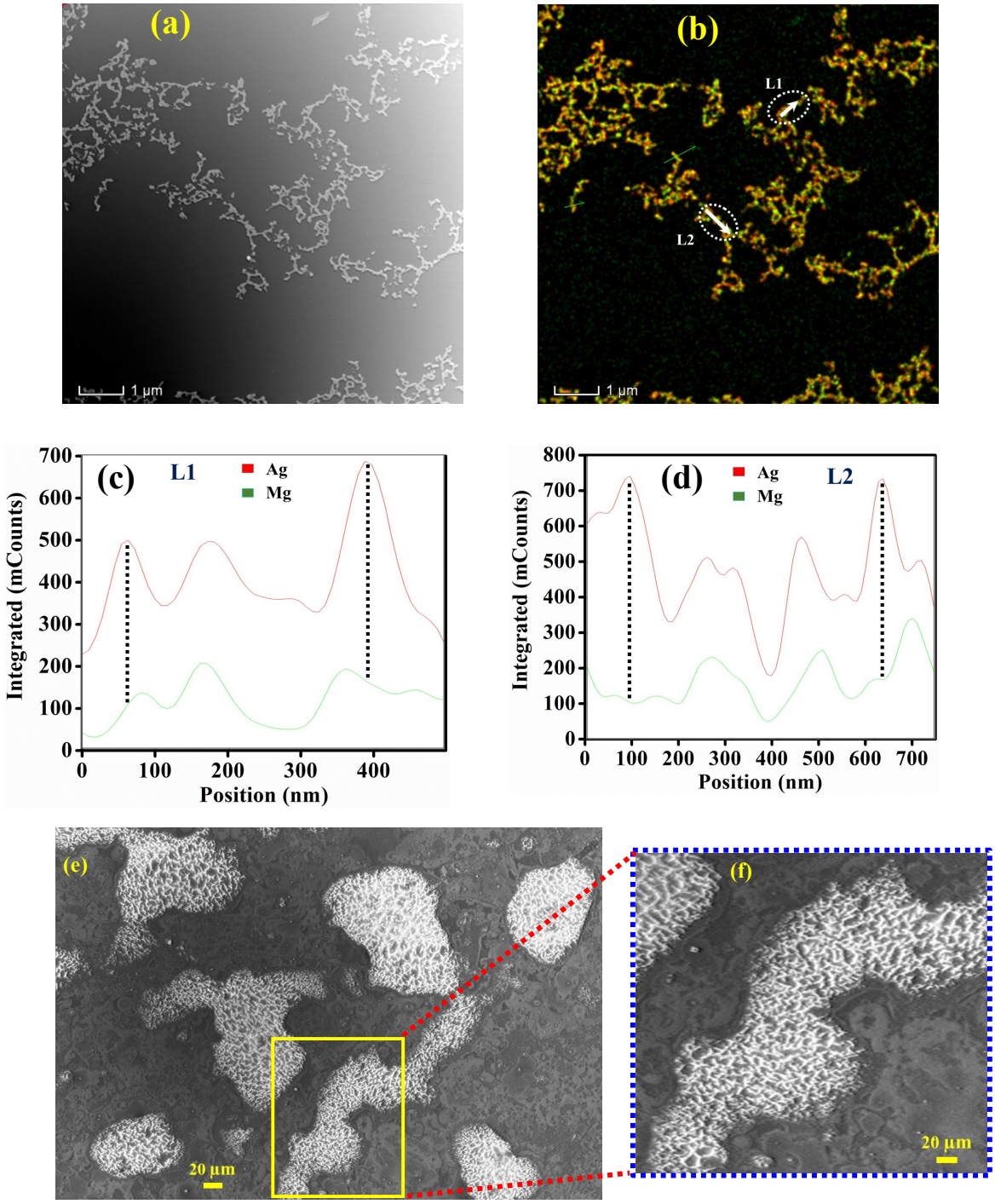

Fig. S3 (a) The bright-field image of Mg-AgNCs shows the highly cross-linking pattern of the nano-assembled structure. (b) Merged elemental mapping of Mg-AgNCs (Ag in red and Mg in green). The corresponding regions of line scanning have also been marked in figure. (c) EDX line-scanning profile of Ag and Mg across the region, L1. (d) EDX line-scanning profile of Ag and Mg across the region, L2. (e) SEM image of Mg-AgNCs displaying the cross-linking pattern. (f) A zoomed-in image of a section of the Mg-AgNCs where the cross-linking pattern is more visible.

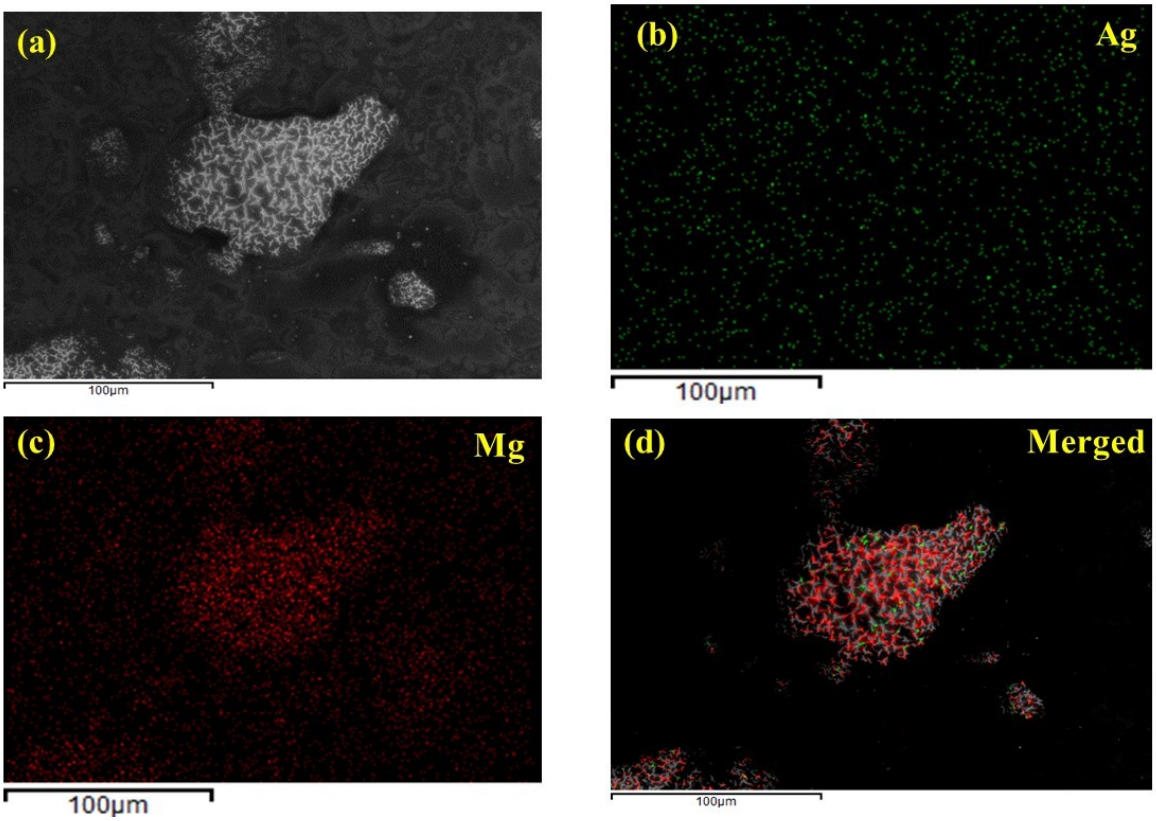

Fig. S4 (a) Bright field SEM image of Mg-AgNCs. Elemental mapping of (b) Ag and (c) Mg and (d) Merged images of Ag and Mg.

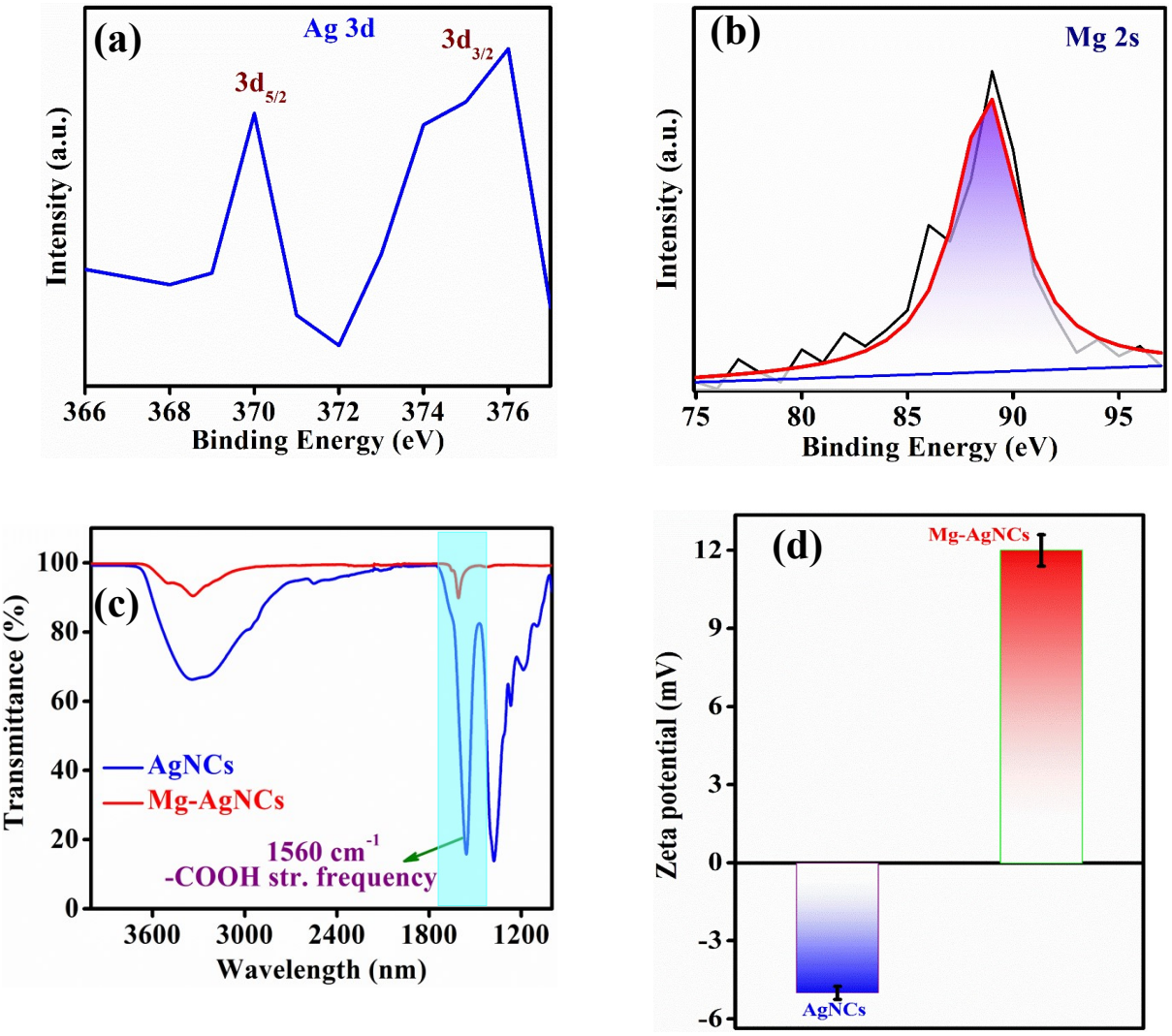

Fig. S5 (a) The XPS spectra of Ag 3d in Mg-AgNCs. (b) The XPS spectra of Mg 2s in Mg-AgNCs. (c) FT-IR spectra of AgNCs and Mg-AgNCs. (d) Zeta potential of AgNCs and Mg-AgNCs representing their surface charges.

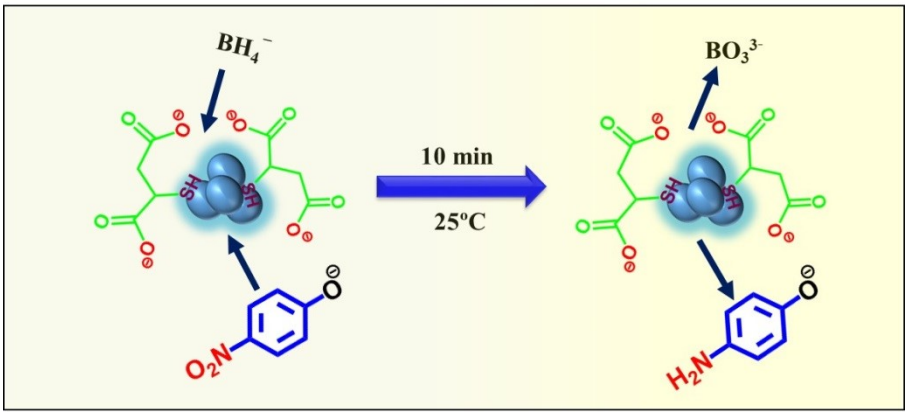

Fig. S6 Plausible schematic representation of 4-NP reduction catalyzed by AgNCs.

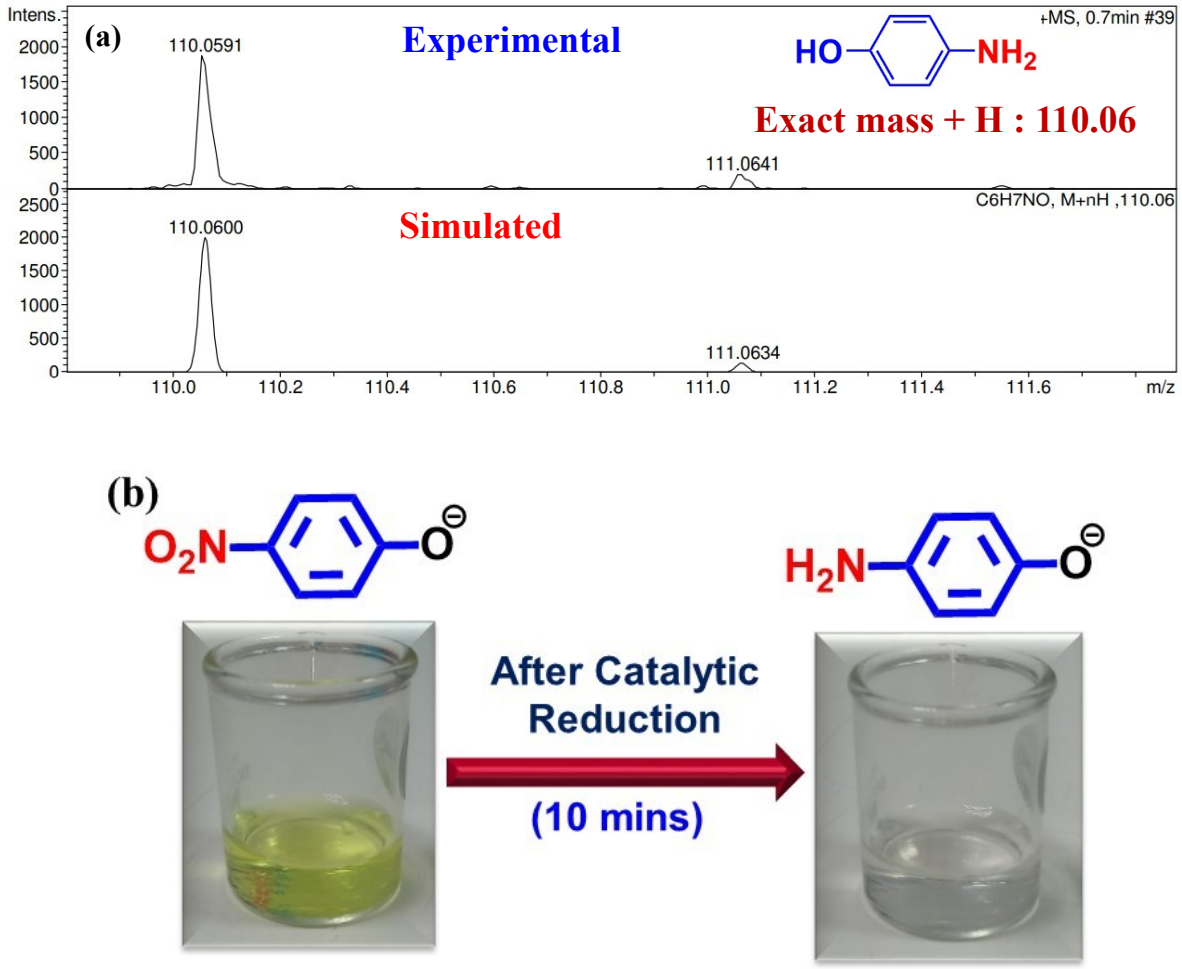

Fig. S7 (a) APCI-MS spectrum of p-aminophenol (4-AP) that was produced by the catalytic reduction of p-nitrophenol (4-NP). (b) Progress of the reaction visualized by the change in colour from light yellow (4-NP) to colourless (4-AP).

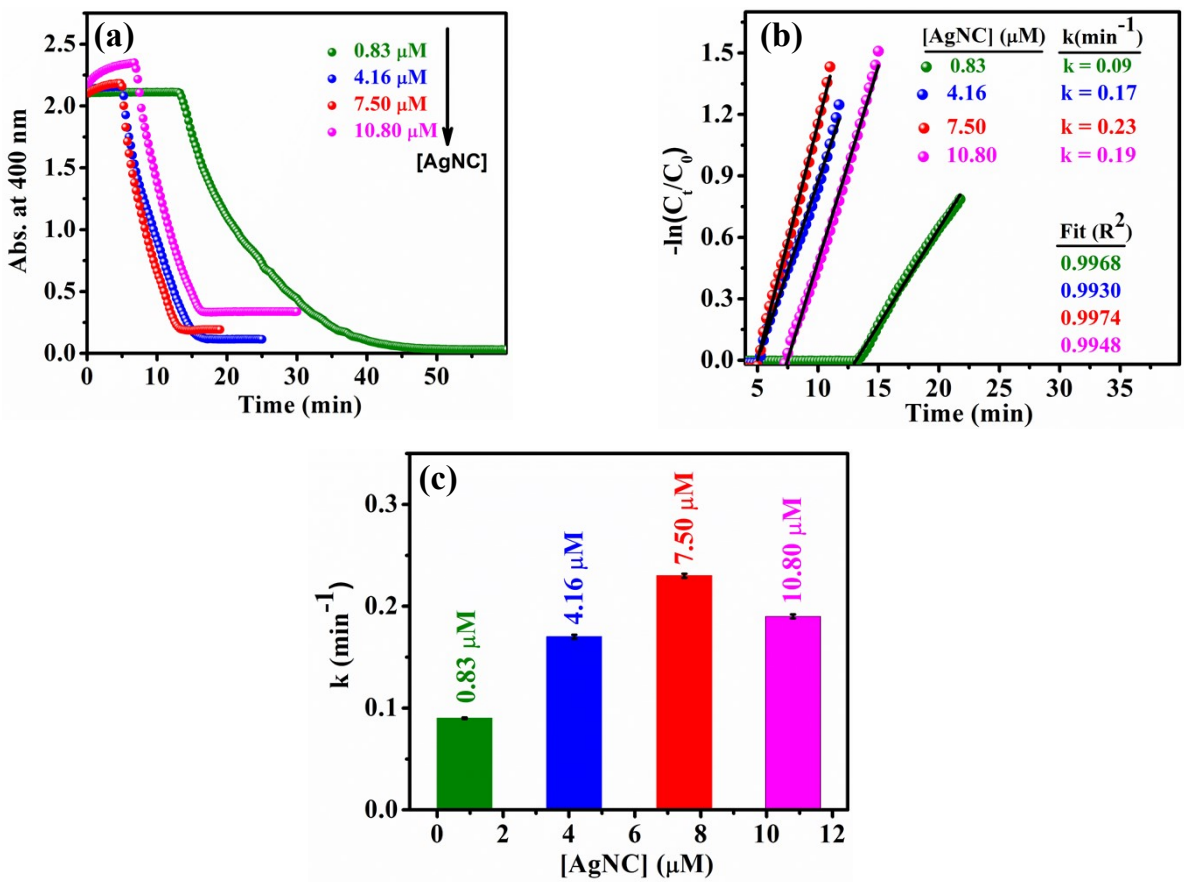

Fig. S8 Optimization of AgNCs for the catalytic process. (a) Changes in absorbance at 400 nm in presence of different concentrations of AgNCs as marked in the Figure. (b) The corresponding linearized data for the first order analysis of rate constants by monitoring the change in absorption at 400 nm with time, at different concentrations of AgNCs. (c) Plot showing the variations in rate constant values at different concentrations of AgNCs.

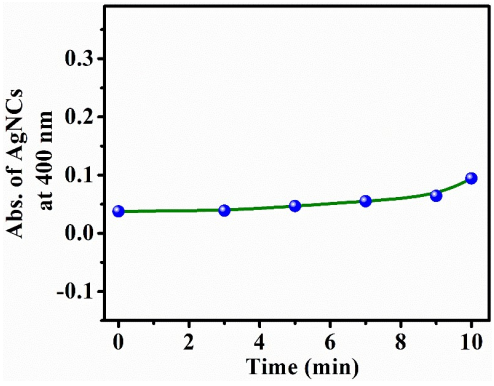

Fig. S9 The change in absorption of AgNCs monitored at 400 nm at different time interval in presence of 10 mM $NaBH_4$.

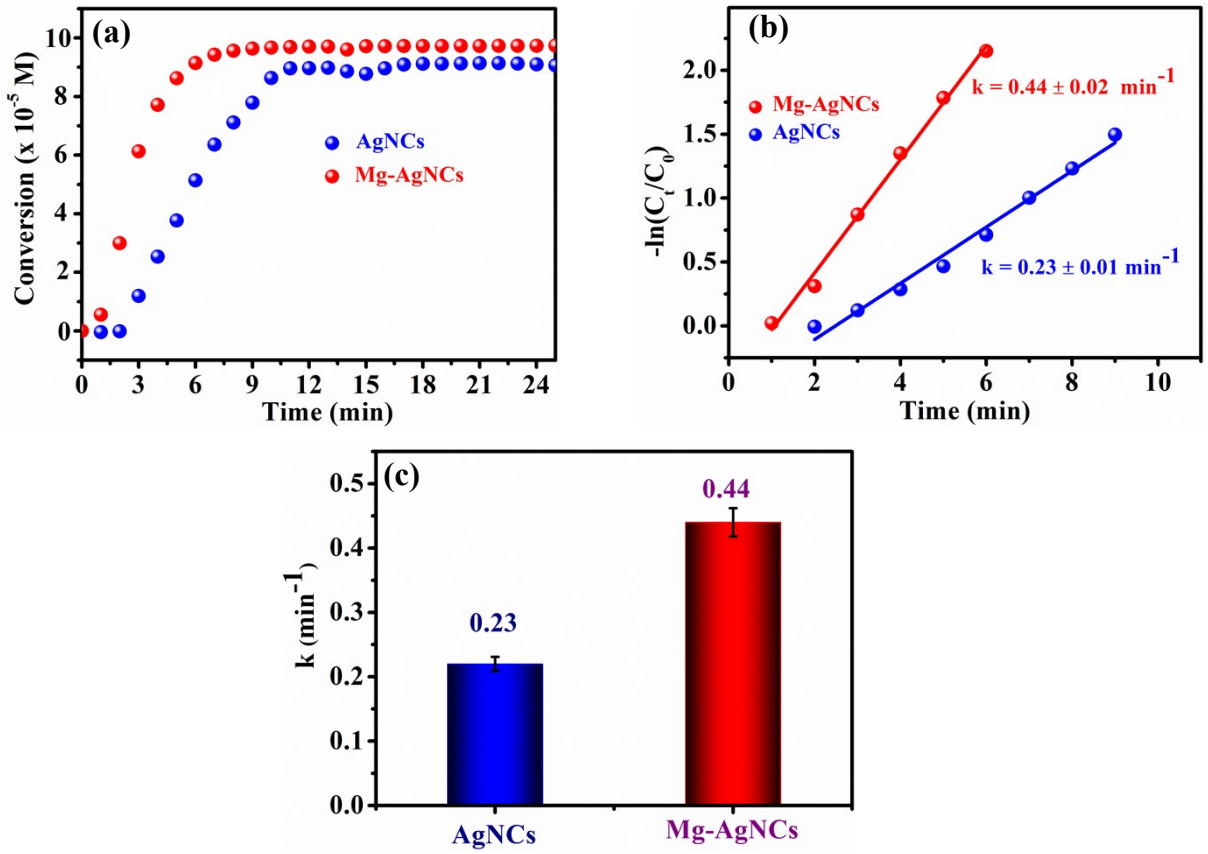

Fig. S10 Influence of Mg^{2+} on 4-NP reduction. (a) Comparison of the extent of conversion to 4-AP (the data is plotted using equation 2). (b) Plot of $-\ln(C_t/C_0)$ *vs* time upon catalytic reduction of 4-NP. The effect of Mg^{2+} ions on the reduction process can be seen herein. (c) Comparison of rate constants for 4-NP reduction between AgNCs and Mg-AgNCs, i.e., in the presence of Mg^{2+} ions.

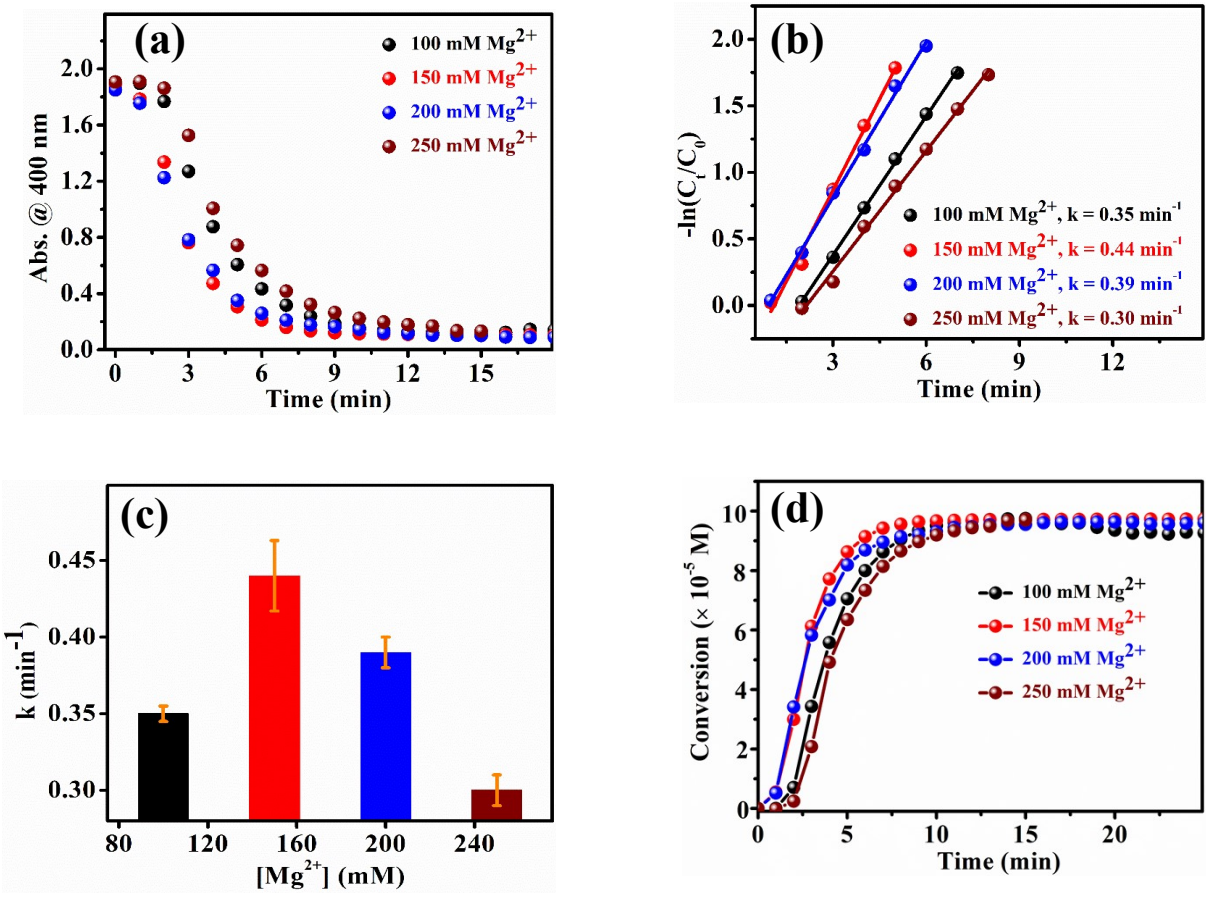

Fig. S11 Optimization of the concentration of Mg^{2+} ions to achieve the best catalytic performance of AgNCs. (a) Changes in absorbance values at 400 nm in presence of different concentrations of Mg^{2+} ions. (b) Plot of $-\ln(C_t/C_0)$ *vs* time upon catalytic reduction of 4-NP in the presence of Mg-AgNCs, with varying concentrations of Mg^{2+} ions. (c) Variation in rate constant values of the reduction reaction at different concentrations of Mg^{2+} ions. The maximum rate constant is obtained for 150 mM Mg^{2+} ions. (d) Change in conversion rate to 4-AP in the presence of various concentrations of Mg^{2+} (the data is plotted using equation 2).

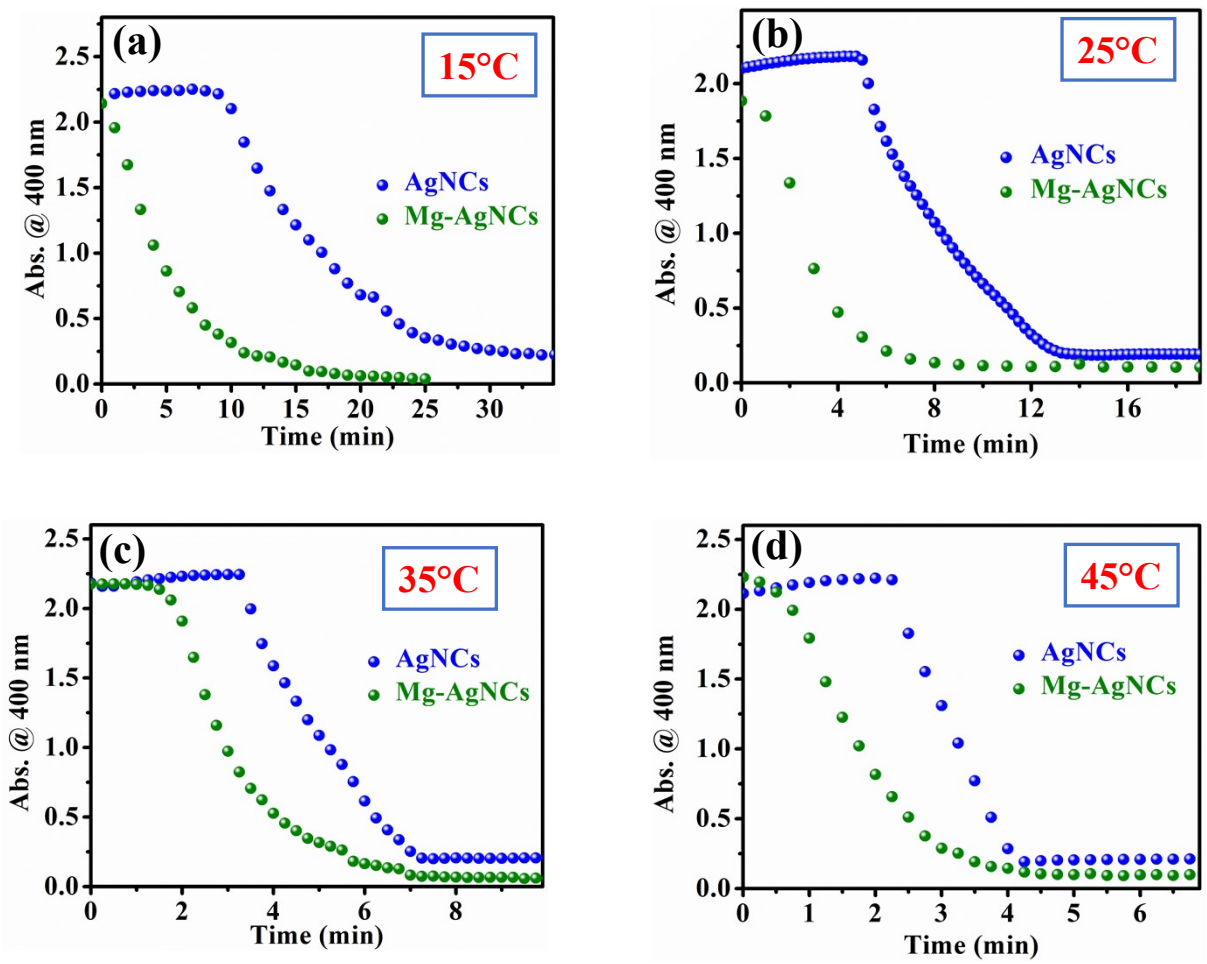

Fig. S12 Temperature-dependent catalytic reduction of 4-NP in the presence of AgNCs and Mg-AgNCs. The progress of the reaction was monitored by tracking the changes in the absorbance at 400 nm in the presence of 7.5 µM AgNCs alone and also in the presence of 150 mM Mg^{2+} ions at different temperatures. (a) 15ºC (b) 25ºC (c) 35ºC and (d) 45ºC.

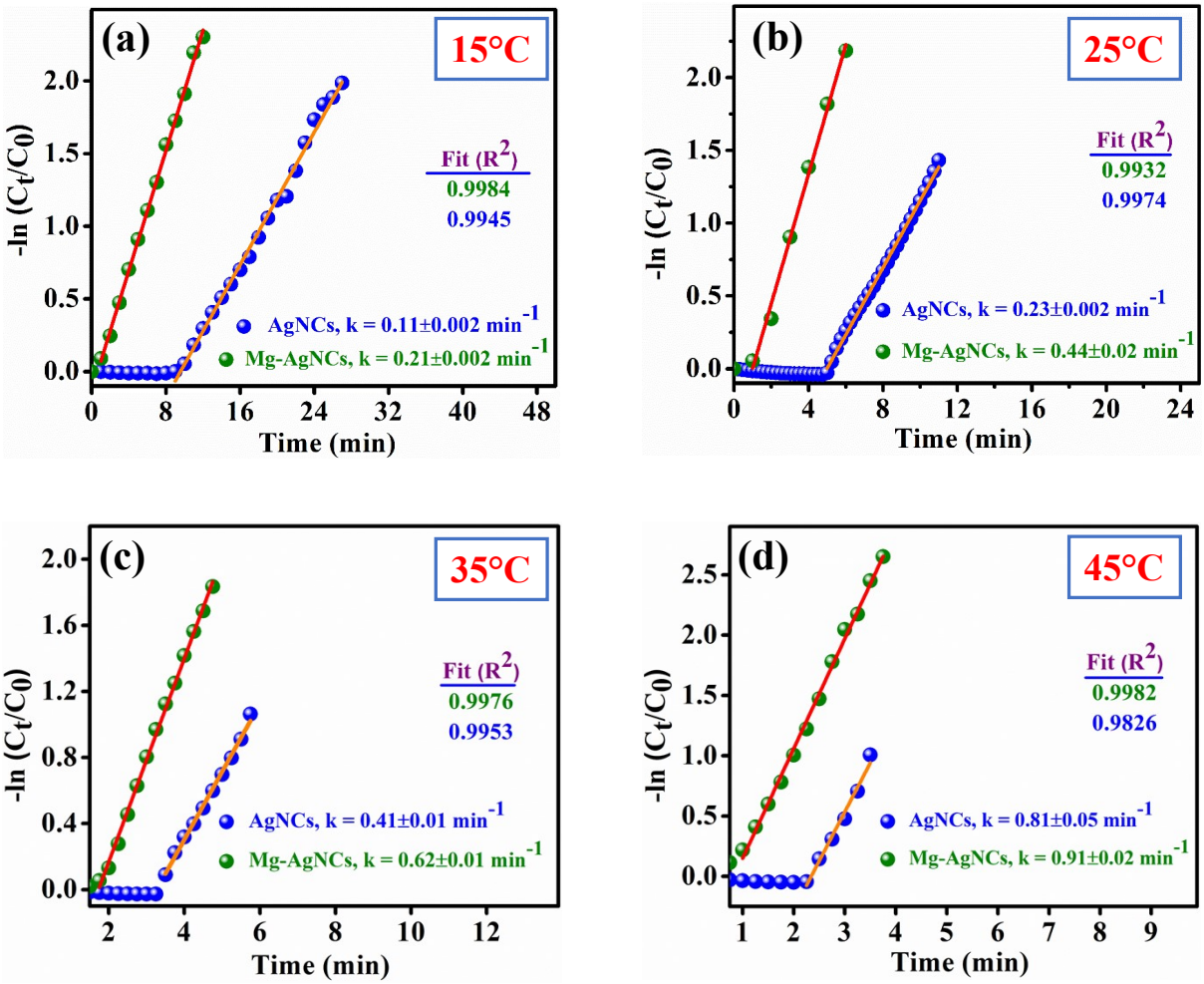

Fig. S13 Temperature-dependent catalytic reduction of 4-NP in the presence of AgNCs and Mg-AgNCs. The linearized data for the first order reaction to evaluate the rate constant of the reaction was obtained by monitoring the change in absorbance at 400 nm in presence of 7.5 µM AgNCs alone and also in the presence of 150 mM Mg^{2+} ions at different temperatures. (a) 15ºC (b) 25ºC (c) 35ºC and (d) 45ºC.

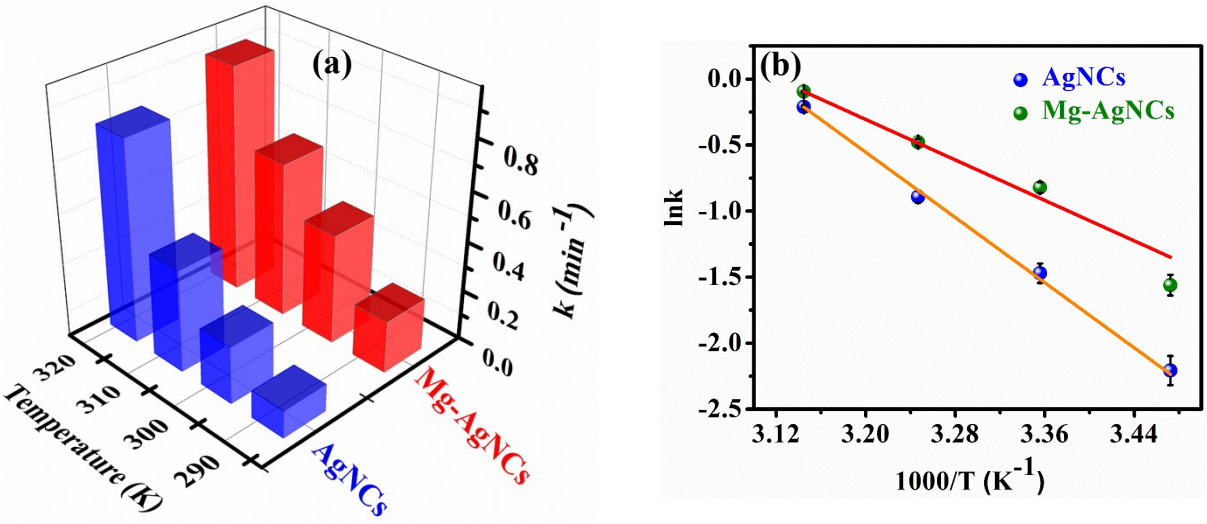

Fig. S14 (a) The variation in the rate constant values for 4-NP reduction as a function of temperature in the presence of AgNCs and Mg-AgNCs. (b) Arrhenius plots to estimate the apparent activation energies associated with the catalytic reaction in the presence of AgNCs and Mg-AgNCs. Here, the concentration of AgNCs and Mg^{2+} in AgNCs were 7.5 µM and 150 mM, respectively.

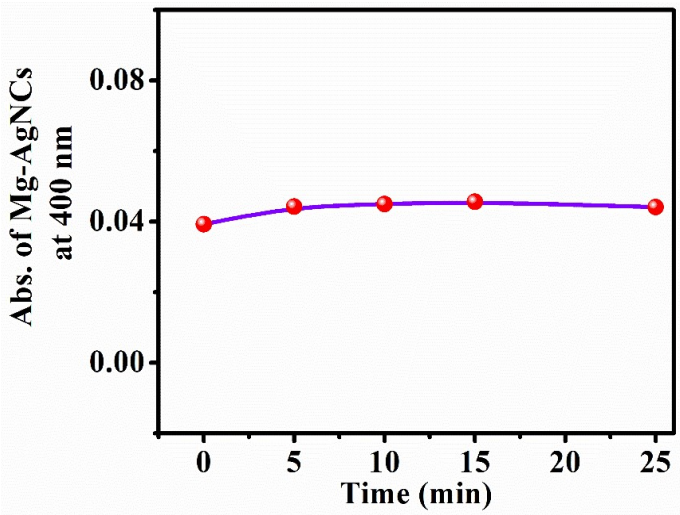

Fig. S15 The change in absorption of Mg-AgNCs monitored at 400 nm at different time intervals in presence of 10 mM $NaBH_4$ used for catalytic reduction.

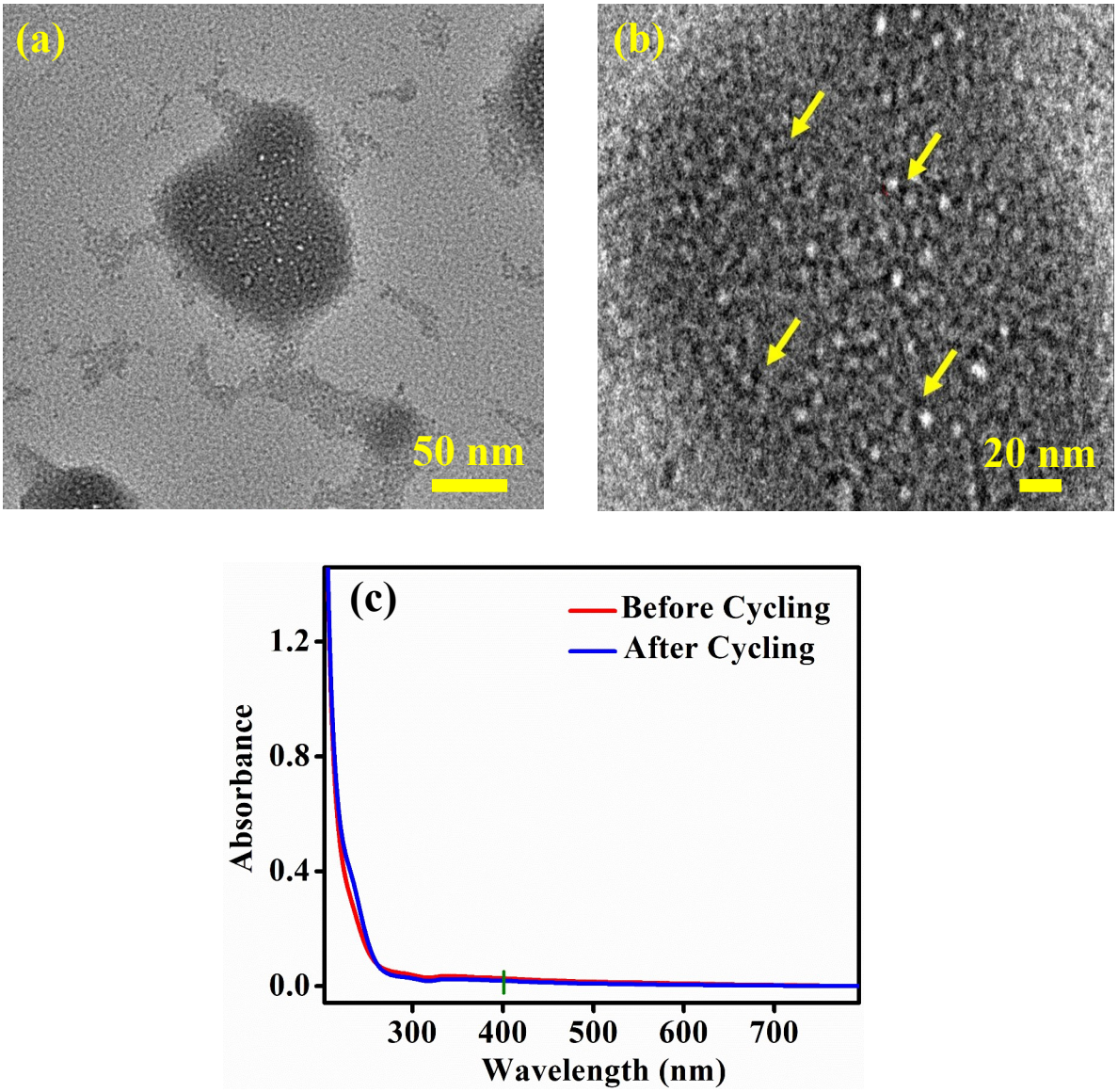

Fig. S16 The TEM images of the Mg-AgNCs after the catalytic reduction reaction. TEM images at (a) 50 nm and (b) 20 nm scale bars, display the preservation of the cross-linked morphologies after the catalytic reaction. (c) The absorption spectra of Mg-AgNCs before and after the catalytic cycle show the stability of Mg-AgNCs during the catalytic cycle.

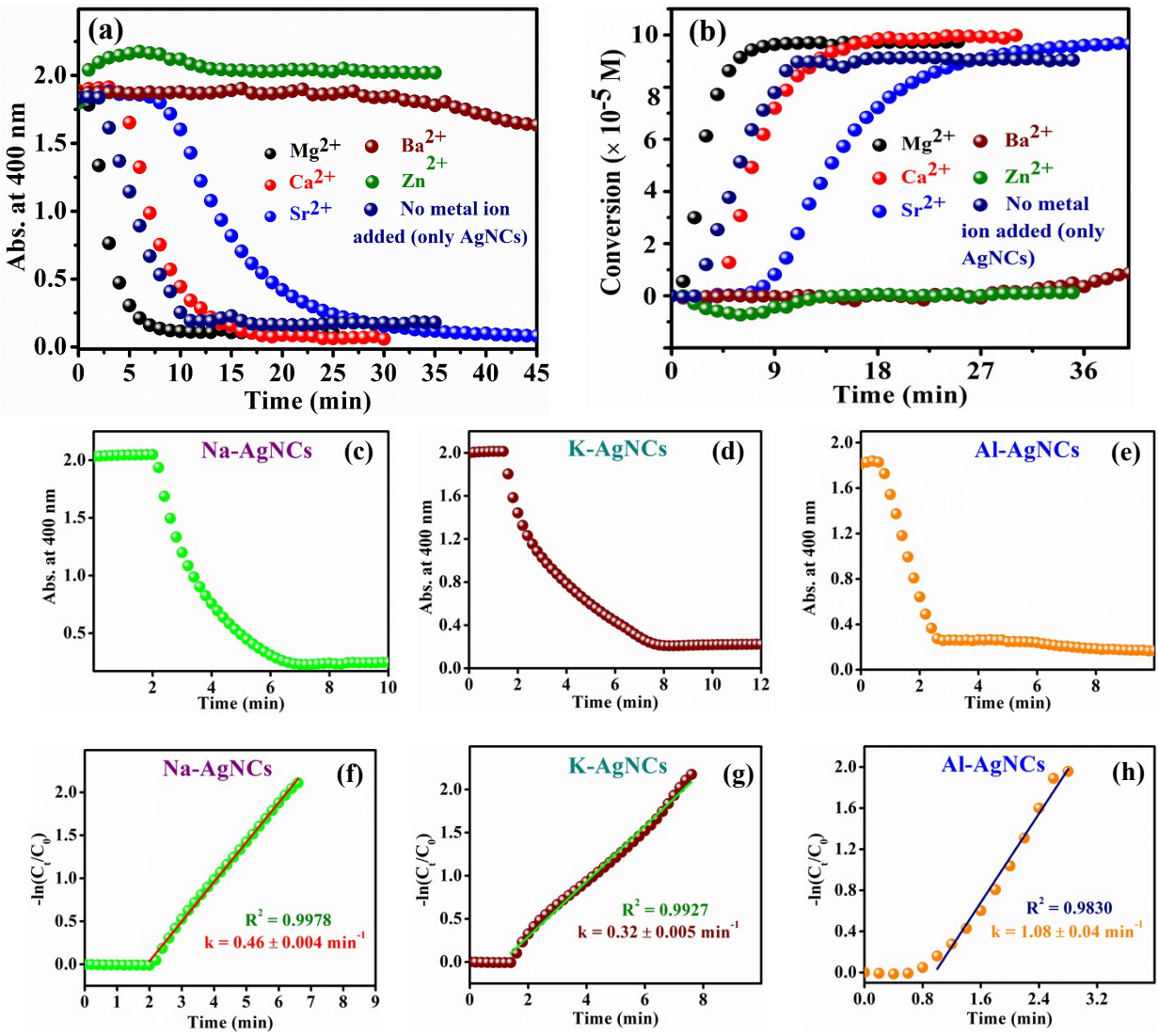

Fig. S17 Impact of different metal ions on the catalytic reduction of 4-NP. (a) Progress of reaction in presence of 150 mM of different metal ions as mentioned in the Figure. (b) Conversion to 4-AP in presence of various metal ions as marked in the Figure. The time-dependent kinetic traces for the reduction of 4-NP catalyzed by AgNCs in presence of (c) Na^+, (d) K^+, and (e) Al^{3+}. The corresponding linearized plots for the estimation of the rate constants in presence of (f) Na^+, (g) K^+, and (h) Al^{3+}. (All metal ions concentrations were kept at 150 mM).

Table S2: Comparison of reaction kinetics with the literature reports for the catalytic reduction of 4-NP.

Catalyst	Catalyst amount	Rate constant (k)	Reference
Au@Ag core-shell NP	3.46 mg/ 25 mL	0.2982 min^{-1} at 298 K	S2
Au NP stabilized with BH_4^-	5 µM	0.12-0.18 min^{-1} at 298 K	S3
Cys@CuNCs	50mg/3mL	0.21 min^{-1} at 298 K	S4
AuNCs@ZIF-8	-	0.489 min^{-1} at 298 K	S5
CPL-AgNCs	-	0.05-0.91 min^{-1} at 297 to 305 K	S6
Cu@MnO_2 Nano-wire	-	571 $S^{-1}g^{-1}$ at 298 K	S7
Cu-W NFs	0.03 mL of 1 mg/mL	0.34 min^{-1} t 298K	S8
Pd@HMSN	50 µL of 1 g/L	0.31 min^{-1} at 298K	S9
Au@RCC3	0.2 mg	0.389 min^{-1} at 298K	S10
AuNPs@MG-SH	-	0.45 min^{-1} t 298K	S11
Mg-AgNCs	**150 mM Mg^{2+} in AgNCs**	**0.44 ± 0.02 min^{-1} at 298 K**	**This work**

Correlation between the ionic strength of the medium and the electrostatic interaction on the reaction kinetics:

The electrostatic interactions play pivotal roles to channelize the catalytic reaction by controlling the surface interactions. The ionic strength of the medium can also influence the extent of electrostatic interactions, and thereby a substantial alteration in the reaction kinetics

is observed. The high ionic strength of the reaction medium minimizes the extent of the electrostatic field induced by the charged surface of the catalyst which in turn impedes the favorable interaction between the catalyst and the substrate, and consequently attenuates the reaction kinetics. The extent of the electrostatic field of a charged particle can be quantitatively ascribed by calculating the Debye screening length which has been depicted below.

Calculations of the Debye screening length (κ^{-1}) for different ionic strengths:

Here, the concentration of the counter ions of Mg-AgNCs is considered to be negligible as compared to 10 mM $NaBH_4$ and PBS buffers (50, 100 mM). This consideration can be rationalized as the prepared Mg-AgNCs were centrifuged rigorously and then the obtained residue of Mg-AgNCs was well re-dispersed in water (discussed in the experimental section). Hence, we can consider that the concentration of the counter ions of Mg-AgNCs is likely to be negligible.

The Debye screening length (κ^{-1}) of an electrostatic field can be calculated by using the following equation:[S12]

$$\kappa^{-1} = \left[\frac{\varepsilon_0 \varepsilon k_B T}{N_A e^2 \sum_i C_i Z_i^2}\right]^{\frac{1}{2}} \qquad (S1)$$

ε_0 = Permittivity of the free space (=8.854 × 10^{-12} m^{-3} Kg^{-1} s^4 A^2)

ε = Dielectric constant of the medium (80 for water)

k_B = Boltzmann's constant

T = Temperature in K (= 298 K), N_A = Avogadro's number, e = charge of the electron (= 1.6 × 10^{-19} C), C_i = concentration of the i^{th} ions (in mol m^{-3}), and Z_i = valency of the i^{th} ions.

The ionic strength of the medium can be expressed as:

$$I = \frac{1}{2}\sum_i C_i Z_i^2 \qquad (S2)$$

Hence, equation (S1) becomes:

$$\kappa^{-1} = \left[\frac{\varepsilon_0 \varepsilon k_B T}{2N_A e^2 I}\right]^{\frac{1}{2}} \qquad (S3)$$

Using equation (S3), Debye screening lengths have been estimated in the media having different ionic strengths and the estimated results have been summarized below:

Table S3: The variation of the Debye screening lengths with the ionic strength of the medium.

	Reaction medium: water	**Reaction medium: 50 mM PBS***	**Reaction medium: 100 mM PBS***
Debye screening length (κ^{-1})	3.07 nm	0.60 nm	0.43 nm

* Equation (S3) has been derived from the Debye-Hückel theory, Normally, it is not applicable for solutions having high ionic strengths (where Debye screening length typically falls into the molecular dimension). However, our estimated values of the Debye screening lengths typically decrease with increasing ionic strength of the medium.

Table S4: The correlation between the ionic strength of the medium and electrostatic interaction for the reduction of 100 μM 4-NP in presence of 10 mM $NaBH_4$ by Mg-AgNCs catalyst. The reaction was carried out in the water and PBS (containing NaH_2PO_4, Na_2HPO_4, and NaCl) medium.

Catalyst	**Zeta potential (mV)**	**Reaction medium**	**Ionic strength of the medium (mol m^{-3})^a**	**Debye screening length (κ^{-1} nm)^b**	**Rate constant (min^{-1}) at 298 K**
Mg-AgNCs	**+12**	Water	10	3.07	0.44 ± 0.02
		50 mM PBS	260	0.60	0.34 ± 0.02
		100 mM PBS	510	0.43	No Catalysis

a calculated using equation (S2)

b calculated using equation (S3)

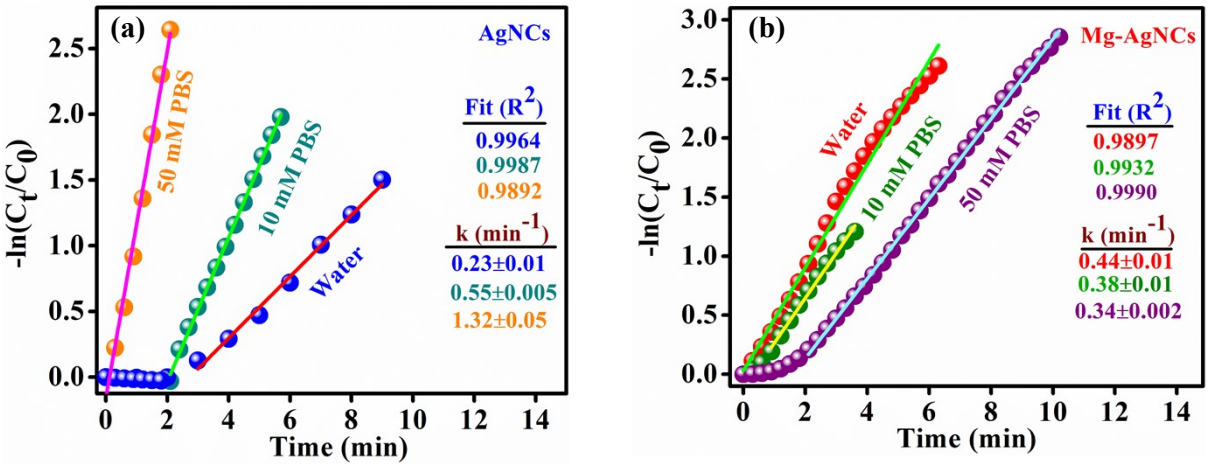

Fig. S18 (a) Linearized plots for the estimation of the rate constants for the reduction of 4-NP using AgNCs as the catalyst, in the presence of different concentrations of PBS, as marked in the Figure. (b) Linearized plots for the estimation of the rate constants for the reduction of 4-NP using Mg-AgNCs as the catalyst, in the presence of different concentrations of PBS, as marked in the Figure. The [4-NP] was kept at 100 μM.

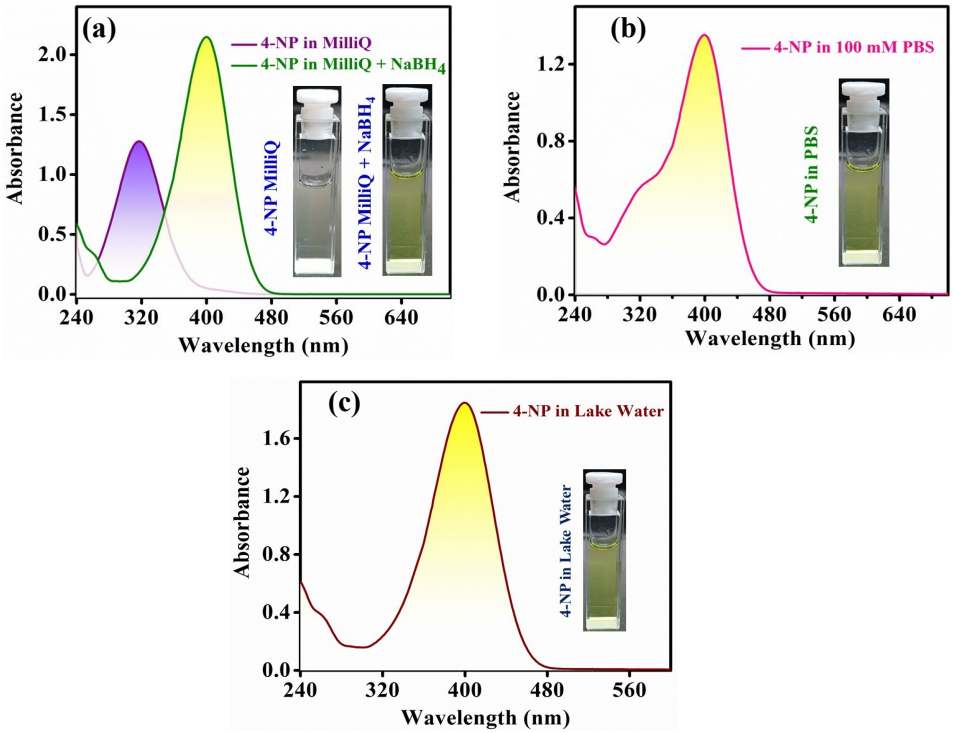

Fig. S19 Absorption profiles of 4-NP in (a) Milli-Q water, (b) PBS, and (c) Lake water. The insets represent the visible color of the solution of 4-NP in different media, as marked in the Fig.s. It must be stated here that the color of 4-NP becomes light yellow due to the formation of 4-nitrophenolate which is clearly visible in the presence of $NaBH_4$, PBS and also in the lake water.

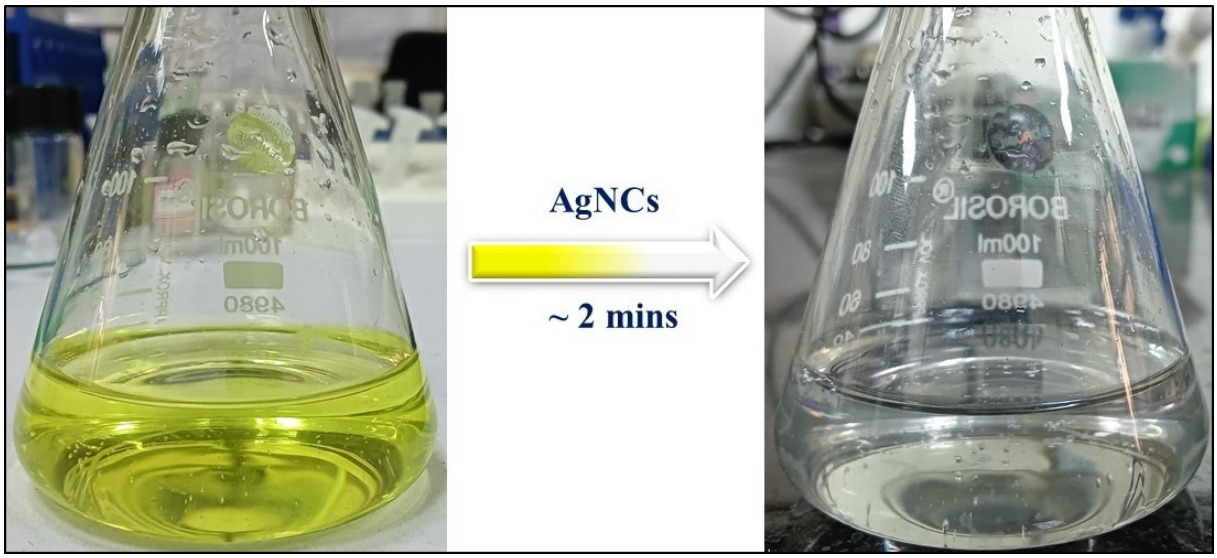

Fig. S20 Real sample analysis in bulk scale with 50 mL reaction volume catalyzed by the AgNCs. [4-NP] = 100 μM.

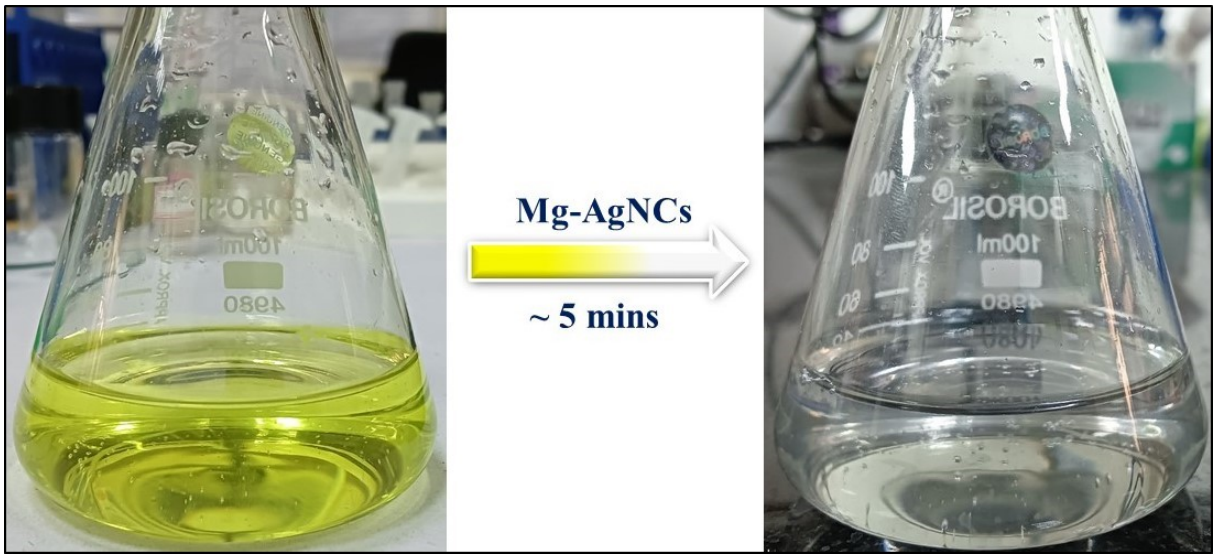

Fig. S21 Real sample analysis in bulk scale with 50 mL reaction volume catalyzed by the Mg-AgNCs. [4-NP] = 100 μM.

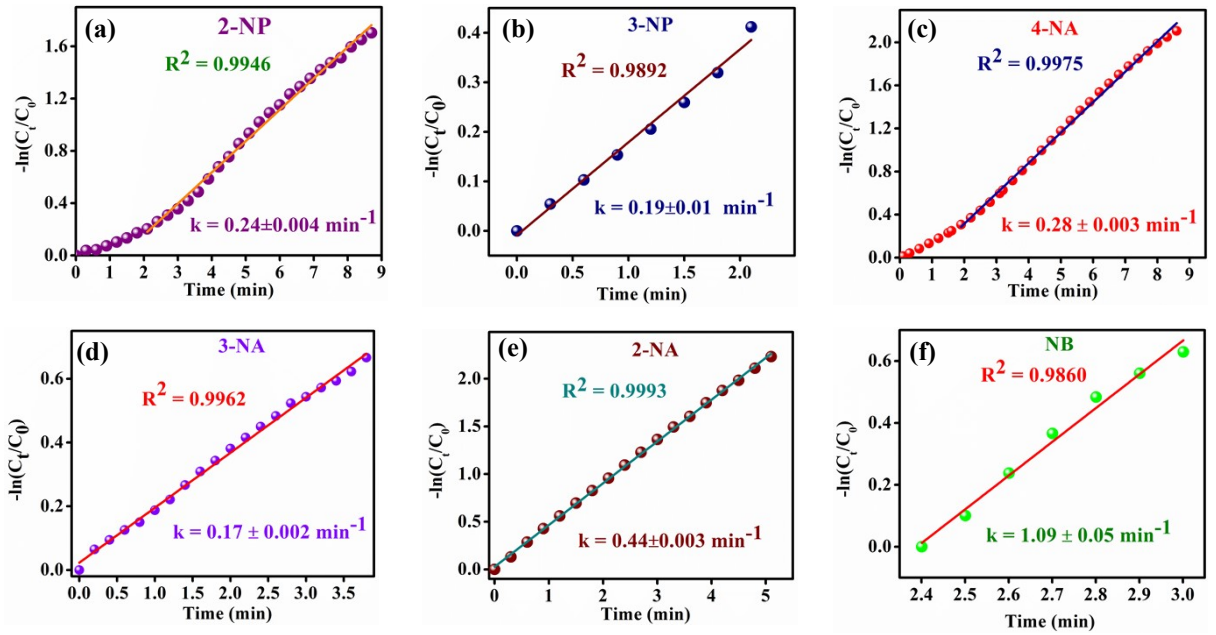

Fig. S22 The linearized plots to evaluate the rate constants for the reduction of (a) 2-NP, (b) 3-NP, (c) 4-NA, (d) 3-NA, (e) 2-NA, and (f) NB.

References:

S1. P. Mahato, S. Shekhar, S. Agrawal, S. Pramanik and S. Mukherjee, *ACS Appl. Nano Mater.*, 2022, **5**, 7571-7579.

S2. H.-L. Jiang, T. Akita, T. Ishida, M. Haruta and Q. Xu, *J. Am. Chem. Soc.*, 2011, **133**, 1304-1306.

S3. E. Menumerov, R. A. Hughes and S. Neretina, *Nano Lett.*, 2016, **16**, 7791–7797.

S4. K. Basu, S. Paul, R. Jana, A. Datta and A. Banerjee, *ACS Sustain. Chem. Eng.*, 2019, **7**, 1998-2007.

S5. G. Gao, Q. Xi, Y. Zhang, M. Jin, Y. Zhao, C. Wu, H. Zhou, P. Guo and J. Xu, *Nanoscale*, 2019, **11**, 1169-1176.

S6. J. Lü, Y. Fu, Y. Song, D. Wang and C. Lü, *RSC Adv*, 2016, **6**, 14247-14252.

S7. C. Du, S. He, X. Gao and W. Chen, *ChemCatChem*, 2016, **8**, 2885-2889.

S8. Y. Ning, Y. Guan, W. Song, F. Zhang, L. Chen and F. Chai, *ChemistrySelect,* 2023, **8***,* e202203194.

S9. X. Huang, D. Lin, P. Duan, H. Chen, Y. Zhao, W. Yang, Q. Pan and X. Tian, *J. Colloid Interface Sci.*, 2022, **629**, 55-64.

S10. Y. Liu, H. Dong, H. Huang, W. Zong, Y.-E. Miao, G. He, I. P. Parkin, F. Lai and T. Liu, *ACS Appl. Nano Mater.*, 2022, **5**, 1276-1283.

S11. K. Chang, Y. Yan, D. Zhang, Y. Xia, X. Chen, L. Lei and S. Shi, *Langmuir*, 2023, **39**, 2408-2421.

S12. S. Roy, A. Rao, G. Devatha and P. P. Pillai, *ACS Catal.*, 2017, **7**, 7141-7145.